Manufacturing Rev. **12**, 11 (2025)

https://doi.org/10.1051/mfreview/2025007

Manufacturing Review
Available online at:
https://mfr.edp-open.org

ORIGINAL ARTICLE OPEN ACCESS

Research on lubrication characteristics of sliding bearings in circular arc gear pumps under variable operating conditions

Shuai Wang[1], Zhenchao Hao[1], Weifeng Han[2], Juntao Liu[3], Geqiang Li[1,*], Yunda Liu[1], and Yiwei Wu[4]

[1] School of Mechatronics Engineering, Henan University of Science and Technology, Luoyang 471003, China
[2] State Key Laboratory of Shield Machine and Boring Technology, Zhengzhou 450001, China
[3] Avic Xinxiang Aviation Industry (Group) Co., LTD, Xinxiang 453700, China
[4] College of Vehicle and Traffic Engineering, Henan University of Science and Technology, Luoyang 471003, China

Received: 22 November 2024 / Accepted: 3 March 2025

Abstract. In response to the problem of lubrication failure of sliding bearings in circular arc gear pumps under variable operating conditions, this paper studies the lubrication characteristics of sliding bearings. Establish a fluid lubrication model for sliding bearings and introduce radial forces and Reynolds boundary conditions. Analyzing the influence of rotational speed and outlet pressure of circular arc gear pump on the lubrication characteristics of sliding bearings based on finite difference method. The research results indicate that as the rotational speed increases, the minimum film thickness gradually increases, the maximum film pressure gradually decreases, and the position of the dynamic pressure effect gradually shifts forward. The maximum film pressure position and the minimum film thickness position differ by about 0.4 rad in the circumferential direction. The acceleration curve has a significant impact on the lubrication characteristics of sliding bearings, and the greater the acceleration, the more obvious the changes in lubrication characteristics. Compared with the acceleration process, the changing trend of lubrication characteristics of sliding bearings during the boosting process is opposite.

Keywords: Circular arc gear pump / sliding bearing / lubrication characteristics / fluid lubrication mode / finite difference method

1 Introduction

Compared with traditional hydraulic systems, direct drive pump controlled hydraulic systems have the advantages of no throttling losses, low energy consumption, and high system integration, and widely used in aerospace and other fields [1–3]. Gear pumps have the characteristics of simple structure, high power density, and strong adaptability [4]. They can not only improve the efficiency and stability of direct drive pump controlled hydraulic systems, but also reduce maintenance and usage costs. With the continuous development of motor technology, the requirements for the performance of gear pumps are also increasing, mainly reflected in the high-speed aspect of gear pumps [5]. Compared with traditional involute gear pumps, circular arc gear pumps have significant advantages in volumetric efficiency and flow pulsation, and there is no trapped oil phenomenon. They have better development prospects in the high-speed development of gear pumps [6]. In a direct drive pump controlled hydraulic system, the regulation of the pump flow rate is achieved through the alteration of the motor speed, which in turn enables the adjustment of the speed, torque, or displacement of the hydraulic motor to facilitate the control of the hydraulic system. Gear pumps usually operate under variable operating conditions, and their rotational speed and outlet pressure change with the operating conditions. However, as a key component of gear pumps, sliding bearings are prone to lubrication failure under variable operating conditions, leading to increased wear of sliding bearings [7]. The evolution of their lubrication performance has not been fully explored [8]. Therefore, to improve the performance and service life of gear pumps in direct drive pump controlled hydraulic systems, research on lubrication of sliding bearings under variable operating conditions has become the key to solving the problem.

Presently, a substantial number of studies on the sliding bearings have been conducted by scholars both within and beyond the academic community. Based on rotor dynamics analysis, Gu et al. [9] analyzed the frictional behavior of sliding bearings using Reynolds boundary lubrication

* e-mail: hitligeqiang@163.com

model and micro convex contact model. Tacconi et al. [10] conducted an analysis of elasto-hydrodynamic lubrication of hybrid sliding bearings in aviation fuel pumps and established an elasto-hydrodynamic lubrication model for aviation gear pumps. Their findings indicate that elastic displacement is a key determinant of oil film pressure distribution. Gu et al. [11] studied the clearance ratio of sliding bearings and analyzed the lubrication characteristics of sliding bearings under different clearance ratios. They found that reducing the clearance ratio and increasing the speed can effectively improve the bearing capacity of sliding bearings. In addition, Xie et al. [12] analyzed the lubrication of UHMWPE bearings under different acceleration and deceleration conditions and found that cosine acceleration was most beneficial for lubrication during the acceleration phase, with the lowest pressure, highest film thickness, and lowest friction coefficient at the same time. Zhang et al. [13] studied the supply pressure of sliding bearings and found that the fluctuation trend of supply pressure is the same as the trend of film thickness change, but opposite to the trend of oil film pressure change. Pressure fluctuations are not conducive to lubrication of sliding bearings. Solghar et al. [14] studied the performance of double groove radial sliding bearings under different load orientations and discovered that an increase in oil supply pressure could reduce the heat. Under high load conditions, it can prevent the occurrence of backflow phenomenon. In summary, current research on sliding bearings mainly focuses on structural parameters and other aspects, analyzing the influence of sliding bearing structural parameters on lubrication characteristics under a certain operating condition. The lubrication characteristics of sliding bearings for non-gear pumps under variable operating conditions have also been studied. However, the lubrication of bearings in gear pumps under variable operating conditions has not been studied in detail.

This article studies the sliding bearings of circular arc gear pumps. The influence of key operating parameters (rotational speed and outlet pressure) of gear pumps on the lubrication characteristics of sliding bearings is numerically analyzed by establishing a fluid lubrication model. In addition, the balance position of the shaft neck under different acceleration curves is studied. The research results provide reference value for the application of gear pumps in direct drive pump controlled hydraulic systems.

2 Material and methods

2.1 Structure and composition

A model of this pump can be seen in Figure 1. Its basic performance parameters are in Table 1. The shaft adopts a double sliding bearing support design, which makes the gear pump work more stably. The driving gear rotates under external force, while the driven gear passively rotates by meshing with the driving gear. Hydraulic oil is sucked in from the inlet and discharged from the outlet. Unlike traditional involute gear pumps, this gear pump has an "arc-sine-arc" rotor end face, which maintains a pair of teeth in meshing state throughout the transmission process, as shown in Figure 2. Therefore, theoretically, there is no trapped oil phenomenon.

The sliding bearing model is shown in Figure 3. To balance the unbalanced radial force generated during operation, the sliding bearing structure adopts a circular oil passage groove and a rectangular static pressure groove structure. The hydraulic oil in the high-pressure chamber first enters the oil passage groove and static pressure groove through the opened oil passage, and then gradually forms a complete oil film, so there is no need to add an additional oil supply device. During operation, the oil at the oil passage groove and static pressure groove forms static pressure and compensates for radial forces, while also supporting the gear shaft. The structural parameters are shown in Table 2.

2.2 Radial force analysis

Radial force generation is a function of two factors, hydraulic pressure and meshing force. Among them, unbalanced circumferential hydraulic pressure is the main cause of radial force generated. From the above analysis, the "arc-sine-arc" tooth profile always keeps a pair of teeth in mesh during the transmission process and does not cause any oil trapping. Therefore, the hydraulic radial force is shown in equation (1).

$$\begin{cases} F_{Px} = \Delta p B R_a \dfrac{\cos\theta_2 - \cos\theta_1}{\theta_2 - \theta_1} \\ F_{Py} = \Delta p B R_a \left(1 - \dfrac{\sin\theta_2 - \sin\theta_1}{\theta_2 - \theta_1}\right) \end{cases}. \tag{1}$$

In equation (1), F_{Px} is the hydraulic pressure in the x-direction; Δp is the pressure difference; B is the tooth width; R_a is the radius of the tooth tip circle; θ_1 is the oil absorption interval angle; θ_2 is the angle of the oil discharge interval; F_{Py} is the hydraulic pressure in the y-direction.

In addition, the mutual meshing between the main and driven gears also generates radial forces, which can be calculated through hydraulic torque. According to mechanical principles, the direction of action of two equal and opposite meshing forces coincides with the meshing line. Therefore, the tangential circumferential force acting on the meshing point is shown in equation (2).

$$F_t = \frac{1}{2R} B\Delta p(R_a^2 - R^2). \tag{2}$$

In equation (2), F_t is the circumferential force; R represents the distance from the meshing point to the center of the main and driven gears.

The main and driven gears are helical, based on the "arc-sine-arc" tooth profile. This ensures continuous transmission of the gear pump. Therefore, the meshing radial force is shown in equation (3).

$$F_r = \frac{1}{2R} B\Delta p(R_a^2 - R^2)\frac{\tan\alpha_n}{\cos\beta}. \tag{3}$$

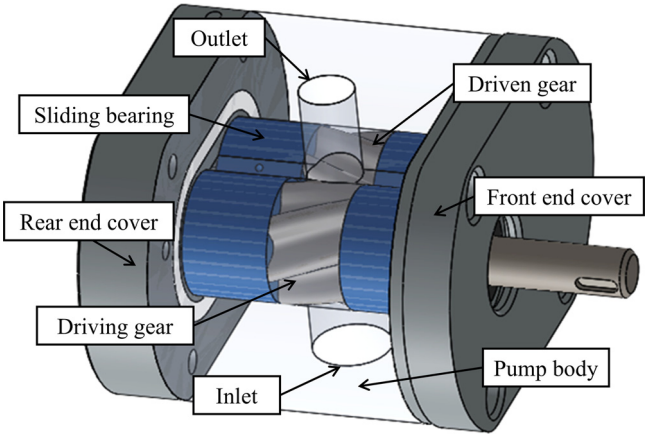

Fig. 1. Structure and composition.

Table 1. Basic performance parameters.

Basic parameters	Parameters value
Outlet pressure (MPa)	15
Output volume (ml/r)	5
Modulus (mm)	3
Tooth number	7
Tooth width (mm)	15.5
Pressure angle (°)	14.5
Helix angle (°)	31.3

In equation (3), F_r, α_n and β are the meshing radial force, pressure angle and helix angle, respectively.

The analysis presented above indicates that hydraulic radial forces on main and driven gears are from outlet to inlet. The meshing radial force of the driven gear is basically the same as the force on the driving gear, equal in magnitude and opposite in direction along the meshing point, as shown in Figure 4. By simplifying and synthesizing the radial force generated by hydraulic pressure and meshing force, the total radial force is shown in equation (4).

$$\begin{cases} F_1 = \sqrt{(F_{Py} - F_t)^2 + (F_{Px} + F_r)^2} \\ F_2 = \sqrt{(F_{Py} + F_t)^2 + (F_{Px} + F_r)^2} \end{cases}. \tag{4}$$

In equation (4), F_1 and F_2 respectively represent the total radial force of the main and driven gears.

The load angles are shown in equation (5).

$$\begin{cases} \beta_1 = \arctan \dfrac{F_{Px} + F_r}{F_{Py} - F_t} \\ \beta_2 = \arctan \dfrac{F_{Px} + F_r}{F_{Py} + F_t} \end{cases} \tag{5}$$

In equation (5), β_1 and β_2 are the load angles of the main and driven gears, respectively.

2.3 Reynolds equation

According to the analysis of radial force, the driven gear experiences greater radial force than the driving gear. Therefore, this article mainly studies the sliding bearings of the driven gear. Make the following assumptions in the analysis: 1. ignore the compressibility of the oil; 2. The gear shaft does not tilt.

Based on the working characteristics of sliding bearings in circular arc gear pumps, the Reynolds equation is given by equation (6).

$$\frac{\partial}{\partial x}\left(ph^3\frac{\partial p}{\partial x}\right) + \frac{\partial}{\partial z}\left(ph^3\frac{\partial p}{\partial z}\right) = 6\mu U\frac{\partial}{\partial x}(ph). \tag{6}$$

In equation (6), x, z, p, h, μ, and U are the lateral coordinate variables, axial coordinate variables, oil film pressure, oil film thickness, hydraulic oil viscosity, and pump rotational speed, respectively.

The film thickness equation serves as the foundation for resolving the Reynolds equation. Assuming the gear shaft is not tilted, the film thickness equation is shown in equation (7).

$$h = c + e\cos\varphi = c(1 + \varepsilon\cos\varphi) \tag{7}$$

In equation (7), c, φ and ε are the radius gap, deviation angle, and eccentricity ($\varepsilon = e/c$), respectively.

Introduce dimensionless variables: $H = h/c$, $P = p/p_0$, $\Lambda = 6\mu R\omega/c^2 p_0$, $\theta = x/r$, $\lambda = z/L$. Among them, p_0, Λ, ω, θ, r, and λ are respectively the ambient pressure, bearing coefficient, angular velocity ($\omega = 2\pi U$), circumferential coordinates, bearing radius, and dimensionless width of the bearing. Equation (8) shows the dimensionless Reynolds equation.

$$\frac{\partial}{\partial\theta}\left(PH^3\frac{\partial P}{\partial\theta}\right) + \frac{4R^2}{L^2}\frac{\partial}{\partial\lambda}\left(PH^3\frac{\partial P}{\partial\lambda}\right) = \Lambda\frac{\partial}{\partial\theta}(PH) \tag{8}$$

2.4 Grid division and solution process

For many practical engineering problems, accurate analytical solutions are generally difficult. With the development of computers and numerical computing technology, numerical methods are now mostly used to solve it. The most used numerical solution method is the finite difference method, which can obtain good calculation results in less computation time.

The dimensionless Reynolds equation is discretized using the finite difference method, after which the successive super relaxation iteration method is employed for the solution. Unfold and divide the oil film pressure bearing area into equidistant grids, with m circumferential grids and n axial grids, as shown in Figure 5. The position of the grid points in the circumferential direction is represented as i, and the position in the axial direction is represented as j, with a total of $m \times n$ grids.

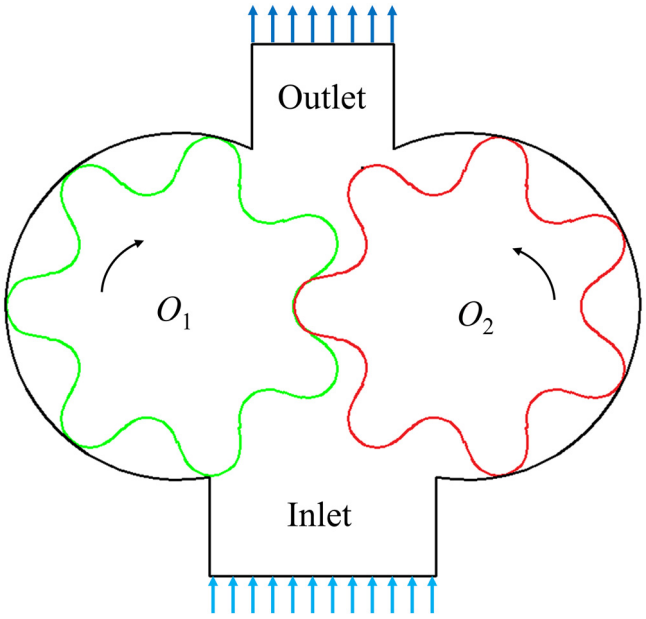

Fig. 2. Transmission process.

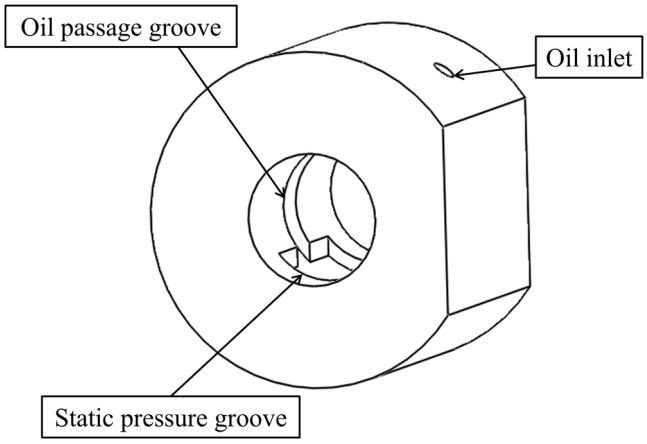

Fig. 3. Sliding bearing mode.

To represent the first derivatives, the center difference quotient formed by the neighboring nodes can be used. To improve the calculation accuracy, this article uses the center difference quotient composed of half step insertion points (Fig. 5) to represent the first derivative. As shown in equation (9) and (10).

$$\left(\frac{\partial P}{\partial \theta}\right)_{i,j} = \frac{P_{i+\frac{1}{2},j} - P_{i-\frac{1}{2},j}}{\Delta\theta} \tag{9}$$

$$\left(\frac{\partial P}{\partial \lambda}\right)_{i,j} = \frac{P_{i,j+\frac{1}{2}} - P_{i,j-\frac{1}{2}}}{\Delta\lambda}. \tag{10}$$

Table 2. Structural parameters of sliding bearing.

Structural parameters	Parameters value
Diameters of the inner diameters of sliding bearing (mm)	14
Width of sliding bearing (mm)	19
Diameters of oil inlet (mm)	1
Angle of oil inlet (°)	45
Width of static pressure groove (mm)	12
Length of static pressure groove sealing oil edge (mm)	2.5
Length of oil passage groove sealing oil edge (mm)	1.5
Depth of groove (mm)	1
Thickness of initial oil film (μm)	30

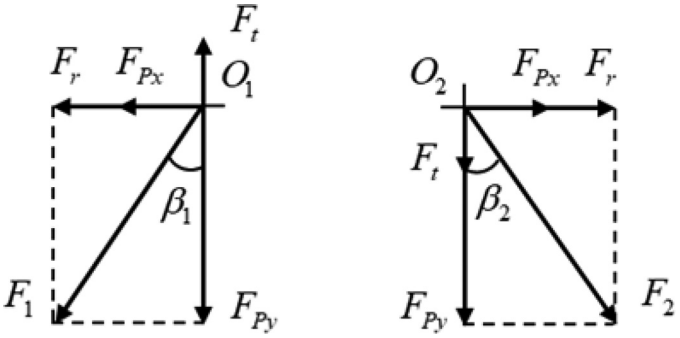

Fig. 4. Radial force analysis.

When solving the second derivative of node (i, j), the center difference quotient of the first derivative of the adjacent half step insertion point can be used first, and then the first derivative can be expressed using the center difference quotient on the corresponding node. As shown in equation (11), (12) and (13).

$$\frac{\partial}{\partial\theta}\left(PH^3\frac{\partial P}{\partial\theta}\right)_{i,j} = \frac{(PH^3)_{i+\frac{1}{2},j}\left(\frac{P_{i+1,j}-P_{i,j}}{\Delta\theta}\right)}{\Delta\theta} - \frac{(PH^3)_{i-\frac{1}{2},j}\left(\frac{P_{i,j}-P_{i-1,j}}{\Delta\theta}\right)}{\Delta\theta} \tag{11}$$

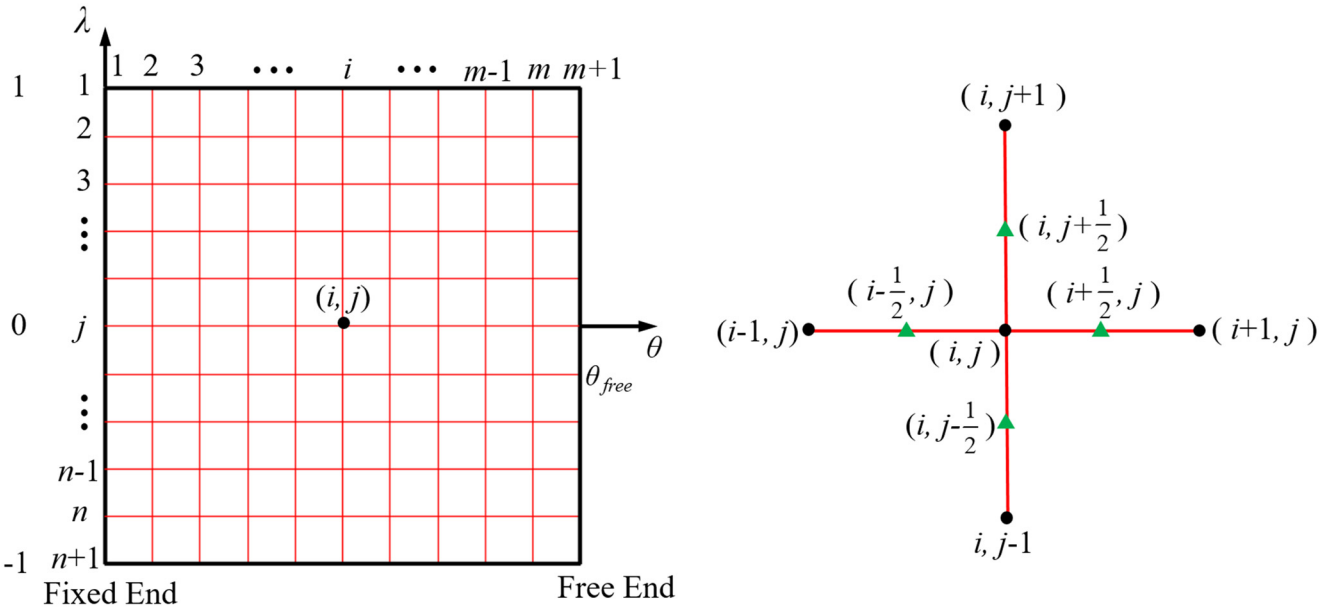

Fig. 5. Oil film grid division and center difference quotient.

$$\frac{\partial}{\partial\lambda}\left(PH^3\frac{\partial P}{\partial\lambda}\right)_{i,j}=\frac{\left(PH^3\right)_{i,j+\frac{1}{2}}\left(\frac{P_{i,j+1}-P_{i,j}}{\Delta\lambda}\right)}{\partial\lambda}-\frac{\left(PH^3\right)_{i,j-\frac{1}{2}}\left(\frac{P_{i,j}-P_{i,j-1}}{\Delta\lambda}\right)}{\partial\lambda} \tag{12}$$

$$\frac{\partial}{\partial\theta}(PH)_{i,j}=\frac{(PH)_{i+\frac{1}{2},j}-(PH)_{i-\frac{1}{2},j}}{\Delta\theta} \tag{13}$$

By substituting equations (9)–(13) into equation (8) for solution, the pressure values of nodes (i, j) are shown in equation (14).

$$P_{i,j}=(AP_{i,j+1}+BP_{i,j-1}+CP_{i+1,j}+DP_{i-1,j}-F)/E \tag{14}$$

The expressions for the corresponding coefficients are shown in equation (15).

$$\begin{cases} A=\dfrac{\left(PH^3\right)_{i+\frac{1}{2},j}}{\Delta\theta} \\ B=\dfrac{\left(PH^3\right)_{i-\frac{1}{2},j}}{\Delta\theta} \\ C=(\dfrac{2R}{L\Delta\lambda})^2\Delta\theta\left(PH^3\right)_{i,j+\frac{1}{2}} \\ D=(\dfrac{2R}{L\Delta\lambda})^2\Delta\theta\left(PH^3\right)_{i,j-\frac{1}{2}} \\ E=A+B+C+D \\ F=\dfrac{\Lambda\left((PH)_{i+\frac{1}{2},j}-(PH)_{i-\frac{1}{2},j}\right)}{\Delta\theta} \end{cases} \tag{15}$$

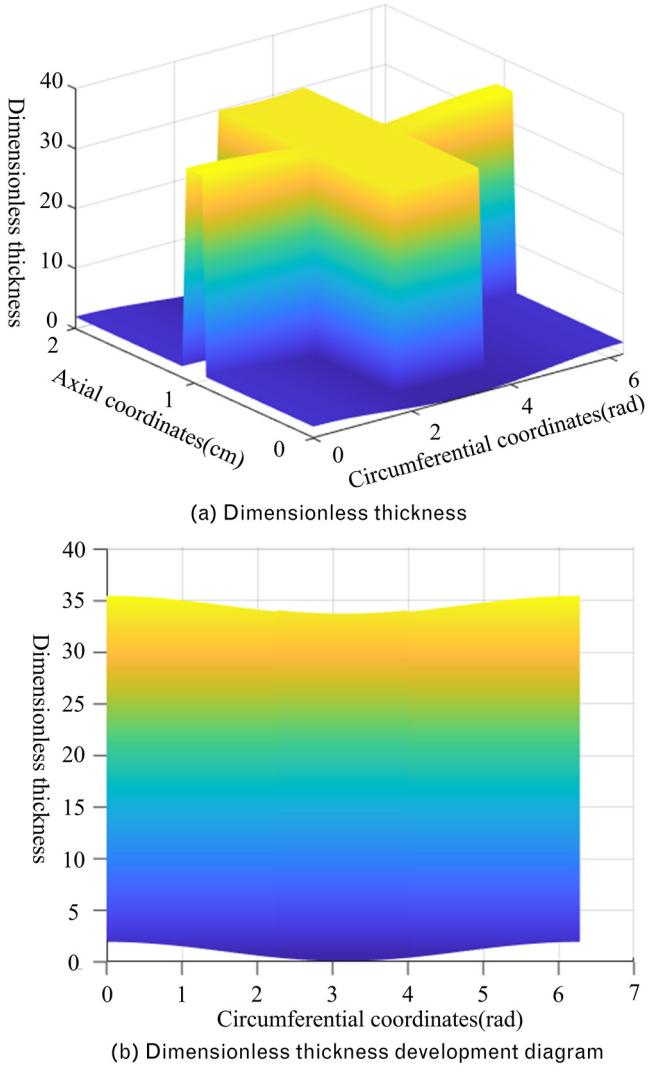

Fig. 6. Oil film thickness.

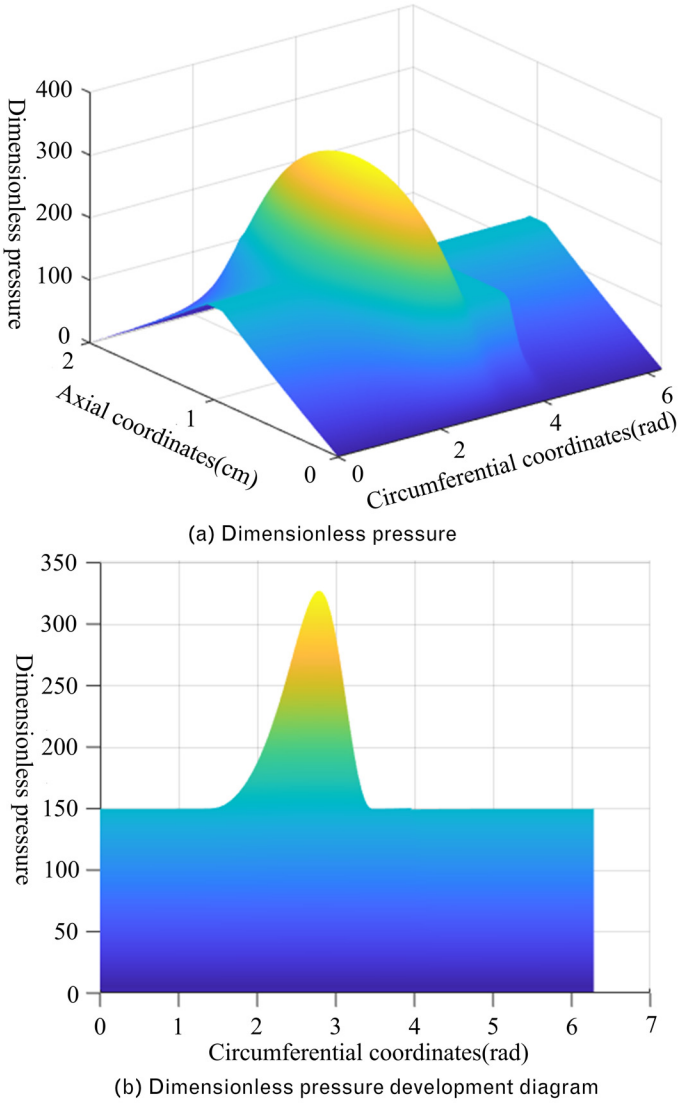

Fig. 7. Oil film pressure.

When solving, the convergence criterion for oil film pressure distribution is shown in equation (16).

$$\frac{\sum_{j=1}^{n+1}\sum_{i=1}^{m+1}|P_{i,j}{}^{(k)} - P_{i,j}{}^{(k-1)}|}{\sum_{j=1}^{n+1}\sum_{i=1}^{m+1}|P_{i,j}{}^{(k)}|} \leq 10^{-5} \tag{16}$$

This article uses MATLAB software for numerical analysis, which can connect different calculation programs and complete complex numerical calculations, while outputting the results as graphical displays. During the calculation process, the first step is to input the structural parameters of the sliding bearing; Secondly, calculate the radial force and introduce it into the calculation model; Then, initial values are assigned to each node in the solution area, Reynolds boundary conditions are introduced, and the iterative method of successive super relaxation is used to solve iteratively. When the convergence criterion is met, the loop is exited; Finally, output information related to the oil film.

3 Results and discussion

3.1 Distribution characteristics of oil film in sliding bearings

Based on the above analysis, numerically solve the fluid lubrication model of sliding bearings. Analyze the distribution characteristics of the oil film in sliding bearings under typical operating conditions of 10000 RPM rotational speed and 15 MPa outlet pressure.

From Figures 6 and 7, the minimum film thickness occurs at the sealing edge of the static pressure groove, and when viewed from the circumferential direction, its position is around 3.1 rad. The maximum film pressure occurs at the static pressure groove, and when viewed from the circumferential direction, its position is around 2.7 rad.

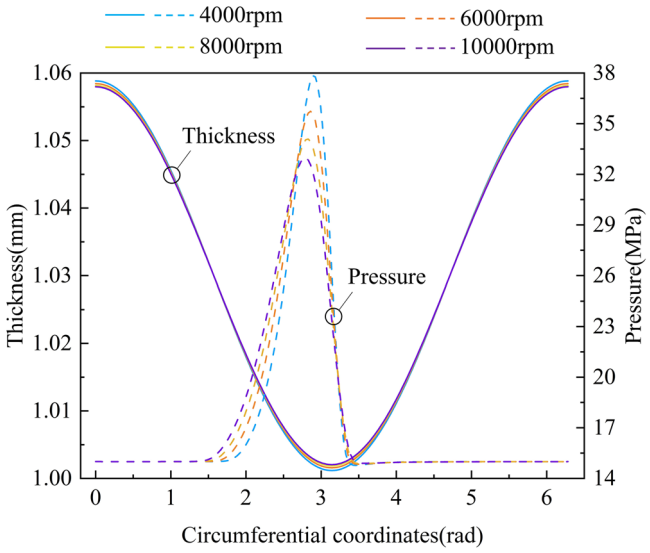

Fig. 8. Distribution characteristics of oil film at the cross-section in the circumferential direction of sliding bearings.

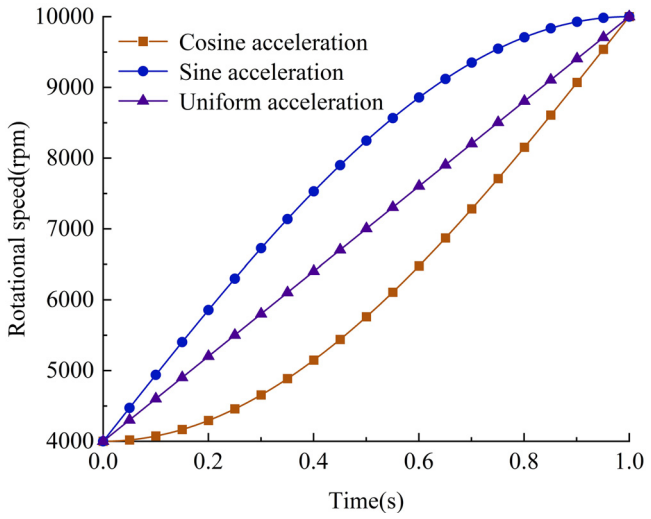

Fig. 10. Rotational speed changes with time in different acceleration modes.

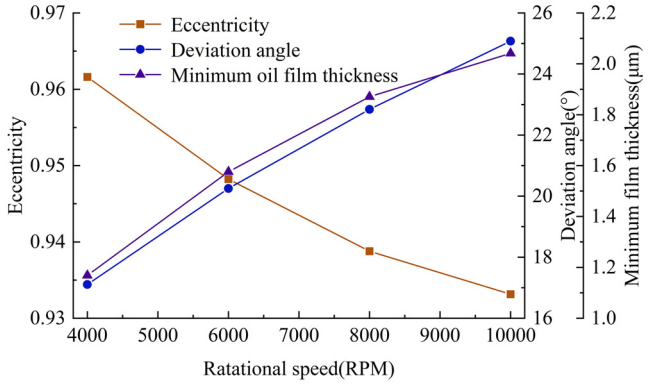

Fig. 9. Changes in the balance position of the shaft neck.

Table 3. Influence of rotational speed on balance position of the shaft neck.

Parameters	Eccentricity	Deviation angle (°)	Minimum oil film thickness (μm)
4000 RPM	0.9616	17.1074	1.1684
6000 RPM	0.9482	20.2505	1.5755
8000 RPM	0.9388	22.8424	1.8705
10,000 RPM	0.9332	25.0764	2.0415

There is a dynamic pressure effect at the starting position of the circumferential angle coordinate of the static pressure groove, and the pressure at the oil passage groove is almost the same. In addition, there is a significant change in film thickness and gradient between the static pressure groove, oil passage groove, and sliding bearing end face, and the film pressure shows a gradually decreasing trend. Both film thickness and pressure show an increasing and then decreasing trend from the axial direction. This is because the sliding bearings of the circular arc gear pump are equipped with oil passage grooves and static pressure grooves. During operation, hydraulic oil reaches the oil passage grooves and static pressure grooves to generate static pressure and support the gear shaft. Under the influence of radial force, the gear shaft is biased towards the direction of the static pressure groove, causing compression on the oil film. Reduce the film thickness while increasing the film pressure under the compression of the gear shaft.

3.2 The influence of rotational speed on bearing lubrication

The oil film distribution characteristics at the circumferential cross-section of the sliding bearing under the same outlet pressure (15 MPa) and different rotational speed conditions are shown in Figure 8. Due to the presence of oil passage grooves and static pressure grooves in sliding bearings, the film thickness is above 1 mm. From the circumferential direction, the maximum film pressure position differs from the minimum film thickness position by about 0.4 rad. From 4000 RPM to 10000 RPM, the maximum film pressure at the cross-section decreased by 4.87 MPa, and the maximum film pressure position gradually moved forward, while the minimum film thickness position remained almost unchanged. As the rotational speed rises, the film thickness at the static pressure groove gradually increases, the film thickness at the oil passage groove gradually decreases, and the starting position of the dynamic pressure effect gradually moves forward. The pressure at the oil passage groove is almost the same as the outlet pressure.

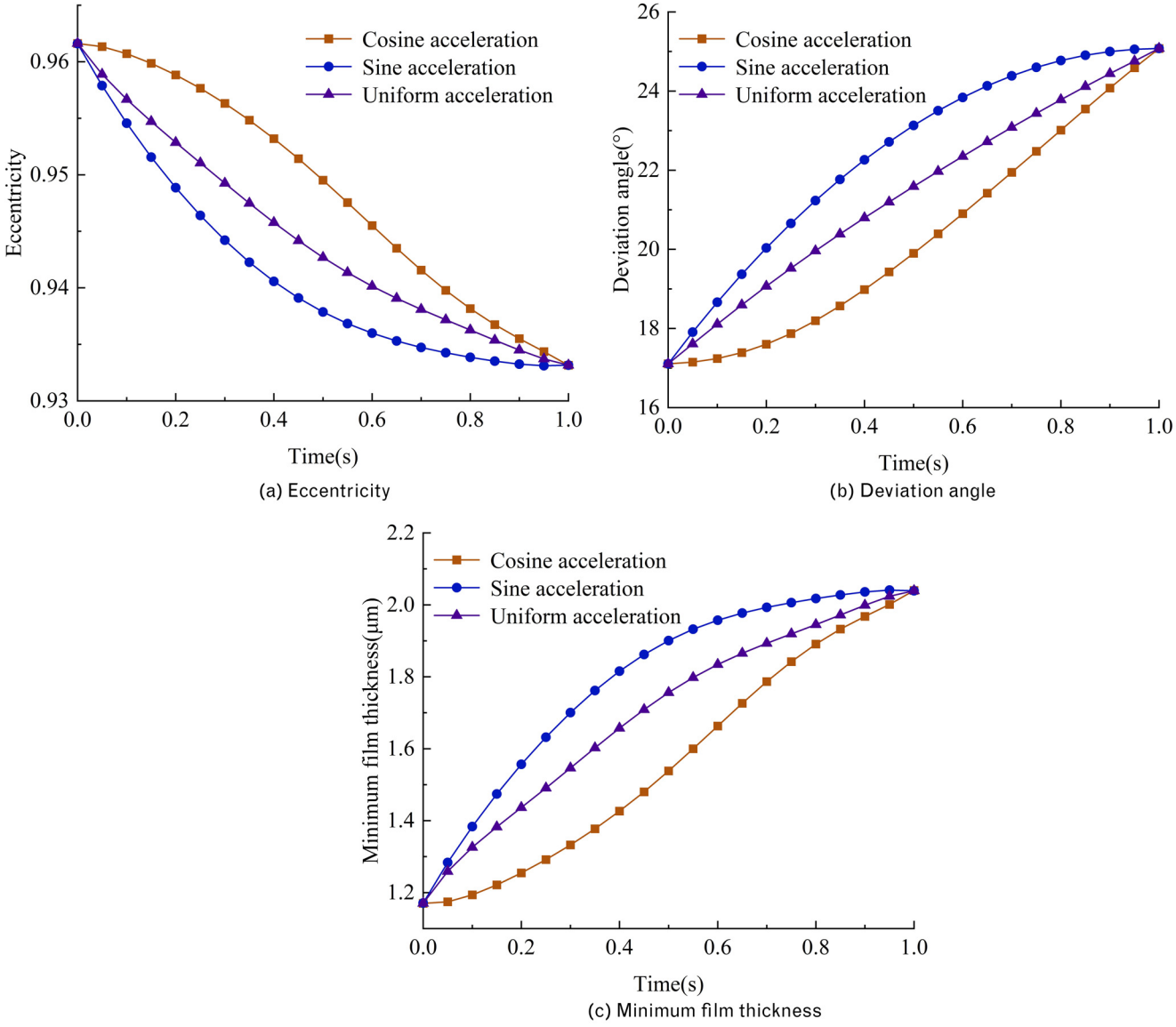

Fig. 11. Changes in the balance position of the shaft neck.

The variation of balance position of the shaft neck at different rotational speeds is shown in Figure 9 and the data are shown in Table 3. With increasing rotational speed, the eccentricity is gradually reduced, while the deviation angle and minimum film thickness are gradually increased. From 4000 RPM to 10000 RPM, the eccentricity decreases by 0.03, the deviation angle increases by 7.97°, the minimum film thickness increases by 0.87 μm, and the balance position of the shaft neck gradually moves towards the center of the sliding bearing. This is because as the rotational speed rises, the starting position of the dynamic pressure effect gradually moves forward, the bearing capacity increases, the offset load decreases, the minimum film thickness increases.

4 The influence of acceleration curve

4.1 Acceleration mode

In practical engineering, uniform acceleration is the most common mode of acceleration. In direct drive pump controlled hydraulic systems, to meet the working requirements and the rigid impact caused by speed changes during uniform acceleration, the acceleration mode is usually changed, such as using sine or cosine acceleration. Figure 10 shows the variation of rotational speed over time under different acceleration modes.

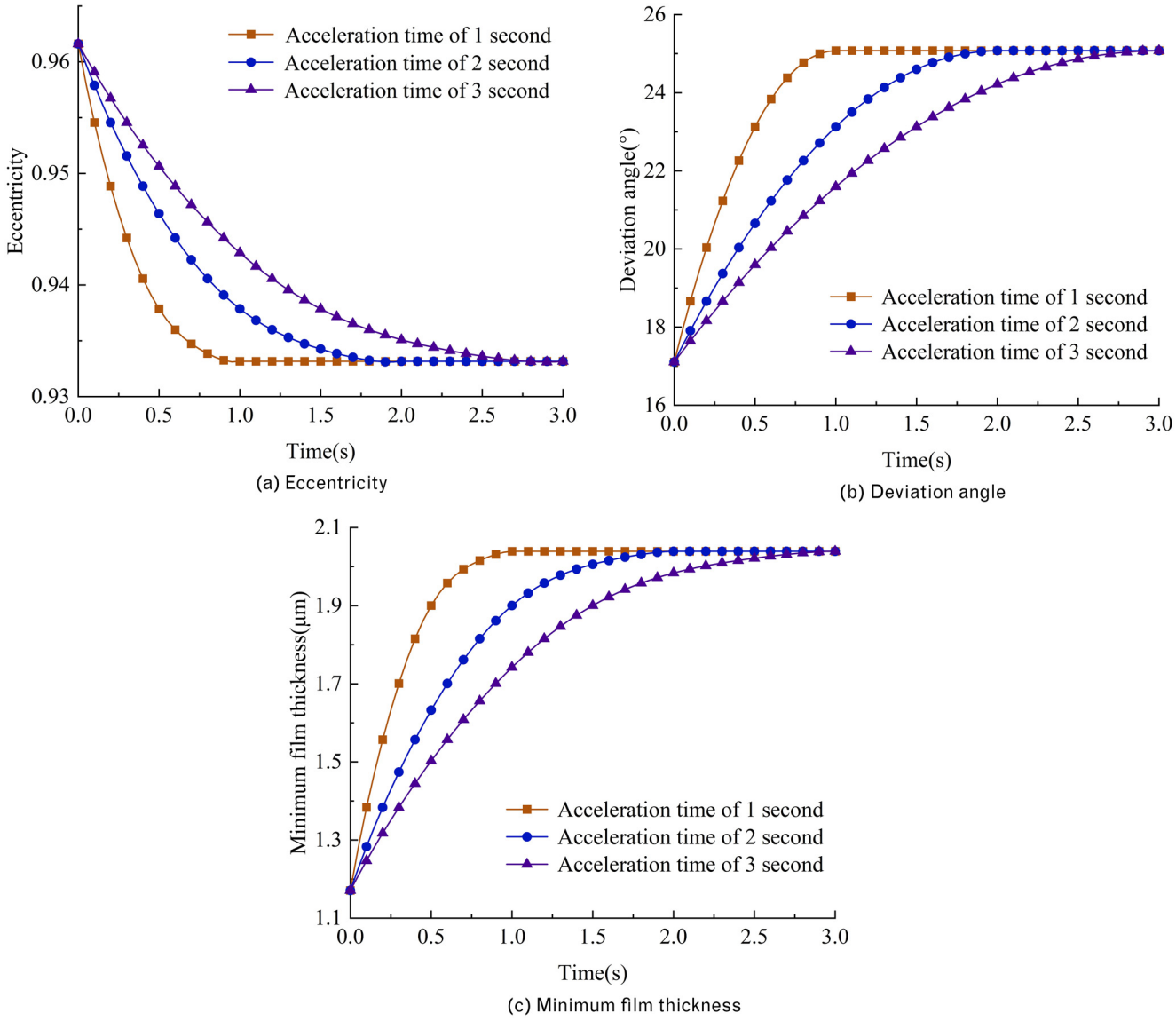

Fig. 12. Changes in the balance position of the shaft neck.

At the same outlet pressure (15 MPa), Figure 11 shows the changes in the balance position of the shaft neck. Acceleration mode is important to change the balance position of the shaft neck; higher acceleration will change in the balance position of the shaft neck more. At the same time, the acceleration modes of eccentricity from high to low are cosine, uniform, and cosine, while the acceleration modes of deviation angle and minimum film thickness from high to low are sine, uniform, and cosine. When entering a steady state, the lubrication characteristics under the sine acceleration mode tend to be smooth, which is more conducive to lubrication of sliding bearings.

4.2 Acceleration time

From the above analysis, the balance position of the shaft neck changes more smoothly under the sine acceleration mode. In this section, the influence of acceleration time on the balance position of the shaft neck is analyzed when the outlet pressure is 15 MPa and the speed is accelerated in a sine mode. Figure 12 shows the changes in the balance position of the shaft neck under the same outlet pressure (15 MPa) and different acceleration times. From 4000 RPM to 10000 RPM, the shorter the acceleration time, the faster the change in the balance position balance position.

4.3 Final rotational speed

When the outlet pressure is 15 MPa and the rotational speed is accelerated in a sine mode, analyze the influence of the final rotational speed on the balance position of the shaft neck. Figure 13 shows the changes in the balance position of the shaft neck at the same outlet pressure (15 MPa) but different final rotational speeds. When accelerating in sine mode, the higher the final rotational speed, the shaft neck balance position and sliding bearing

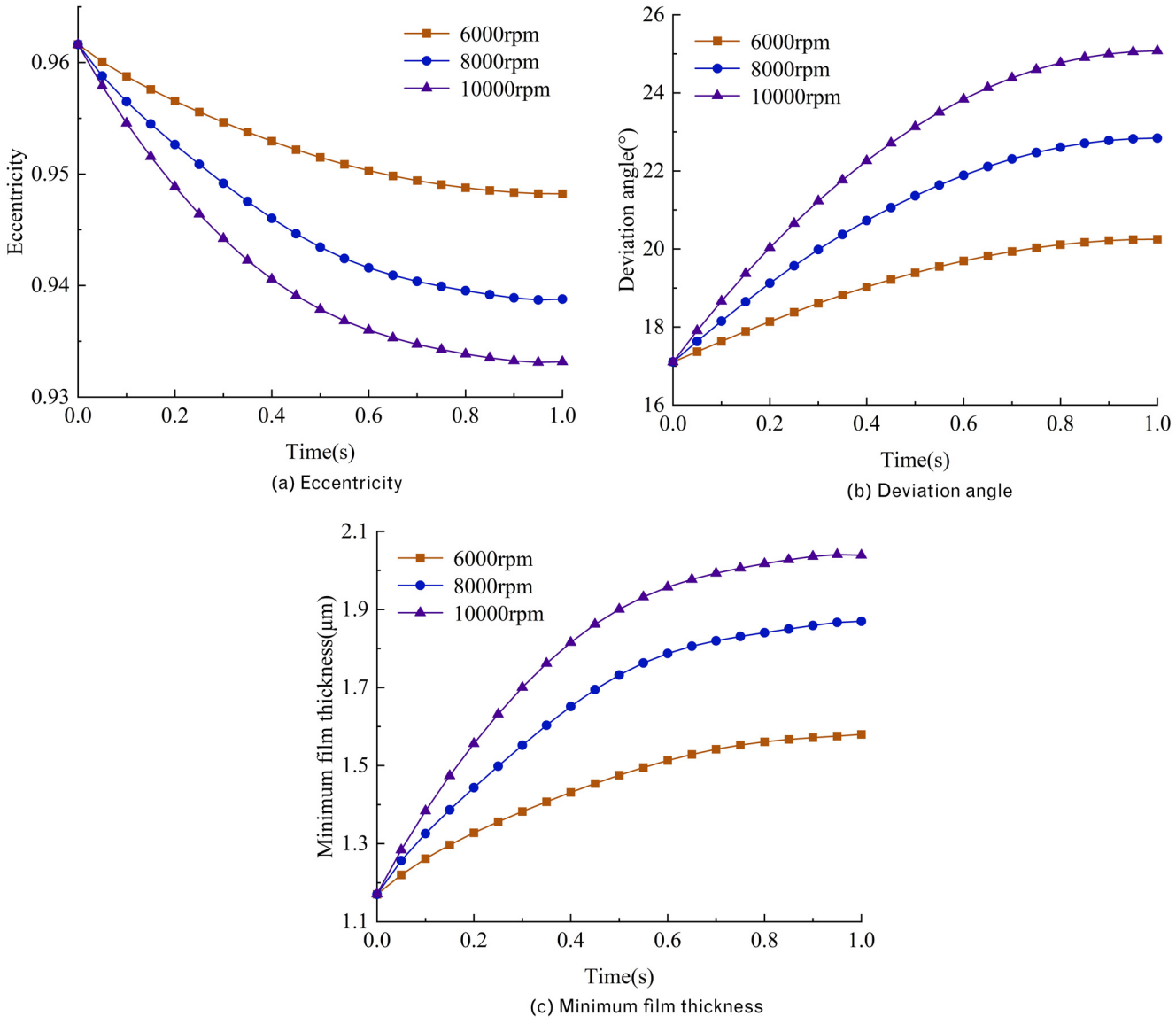

Fig. 13. Changes in the balance position of the shaft neck.

center are closer together, reducing the possibility of friction between the shaft neck and the sliding bearing, and improving the bearing's lubrication performance.

5 The influence of outlet pressure on bearing lubrication

The distribution characteristics at the circumferential cross-section of the sliding bearing under different pump outlet pressures at the same rotational speed (10000 RPM) are shown in Figure 14. When the outlet pressure increases from 5 MPa to 15 MPa, the maximum film pressure at the cross-section increases by 23.71 MPa, and the maximum film pressure position is progressively advanced, while the minimum film thickness position remained almost unchanged. With increasing outlet pressure, there is a gradual reduction in static pressure groove filming, a gradual increase in oil passage groove filming, and a gradual backward shift in dynamic pressure effect. The film pressure at the oil passage groove hardly changes and is consistent with the trend of changes in pump outlet pressure. Compared to rotational speed, outlet pressure has a greater impact on bearing lubrication.

The variation of balance position of the shaft neck at different rotational speeds is shown in Figure 15 and the data are shown in Table 4. Compared with the acceleration process, the impact trend of the boosting process on the balance position of the shaft neck is opposite. The eccentricity increases by 0.25, the deviation angle decreases by 12.69°, the minimum film thickness decreases by 7.54 μm and the balance position of the shaft neck gradually deviates from the center of the sliding bearing

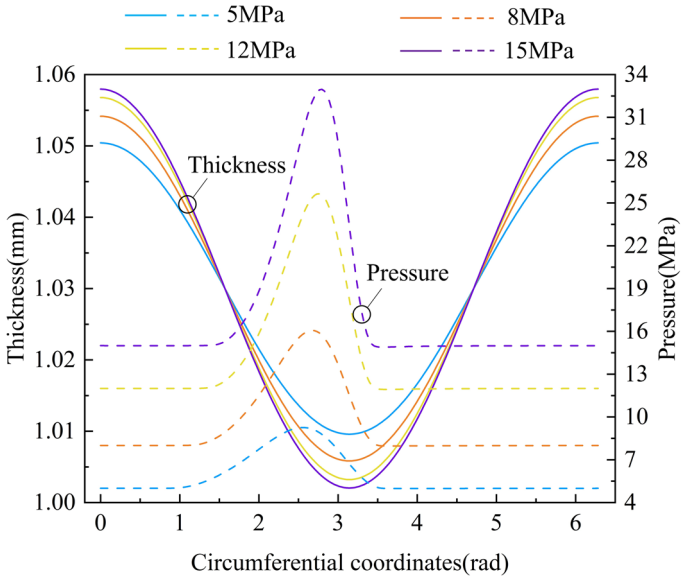

Fig. 14. Distribution characteristics of oil film at the cross-section in the circumferential direction of sliding bearings.

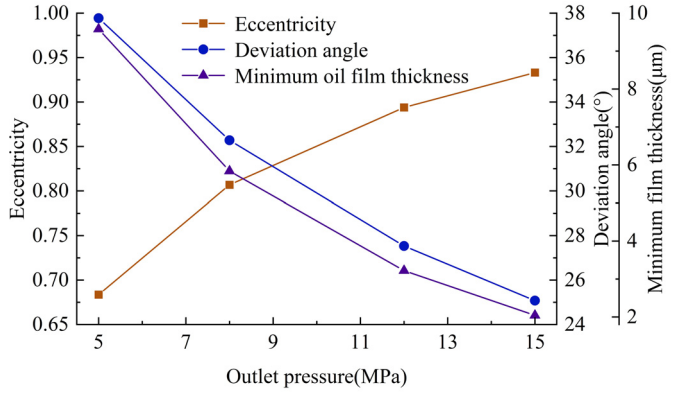

Fig. 15. Changes in the balance position of the shaft neck.

Table 4. Influence of outlet pressure on balance position of the shaft neck.

Parameters	Eccentricity	Deviation angle (°)	Minimum oil film thickness (μm)
5 MPa	0.6836	37.7728	9.5801
8 MPa	0.8069	32.28	5.8359
12 MPa	0.8938	27.5311	3.2207
15 MPa	0.9332	25.0764	2.0415

as the output pressure increases from 5 MPa to 15 MPa. This is because as the outlet pressure increases, the oil supply pressure and radial force also increase, the gear shaft's squeezing effect on the oil film increases and minimum film thickness decreases.

6 Conclusion

Based on the equations of motion and continuity of incompressible fluid, a fluid lubrication model of sliding bearings of circular arc gear pumps is established, and radial force and Reynolds boundary conditions are introduced. The bearing lubrication characteristics under different working conditions are analyzed. The fluid lubrication model assigns an initial value to each node in the solution region, and the solution is carried out using the super relaxation iteration method, and the results are obtained by means of numerical solution to simulate the lubrication characteristics and change trend of the oil film of the sliding bearing, to provide a theoretical basis and guidance for the optimal design of the sliding bearing structure, and to provide a reference value for the application of the gear pump in the direct-drive pump-controlled hydraulic system.

The minimum film thickness appears at sealing edge of the static pressure groove, and when viewed from the circumferential direction, its position is around 3.1 rad; The maximum film pressure occurs at the static pressure groove, and when viewed from the circumferential direction, its position is around 2.7 rad. There is a dynamic pressure effect at the starting position of the circumferential angle coordinate of the static pressure groove, and the pressure at the oil passage groove is almost the same. Both film thickness and pressure show an increasing and then decreasing trend from the axial direction.

With increasing rotational speed, the film thickness at the static pressure groove gradually increases, the film thickness at the oil passage groove gradually decreases. The starting position of the dynamic pressure effect gradually moves forward, while the minimum film thickness position remains almost unchanged. The maximum film pressure at the cross-section decreases by 4.87 MPa and the balance position of the shaft neck gradually moves towards the center of the sliding bearing when the rotational speed increases from 4000 rpm to 10,000 rpm. The acceleration curve has a significant impact on bearing lubrication. The greater the acceleration, the greater the change in the balance position of the shaft neck.

As the outlet pressure increases, the static pressure groove film thickness gradually decreases, while the oil passage groove film thickness gradually increases. The maximum film pressure position gradually moves forward, the starting position of the dynamic pressure effect gradually moves backward, and the minimum film thickness position remains almost unchanged. When the outlet pressure increases from 5 MPa to 15 MPa, the maximum film pressure at the cross-section increases by 23.71 MPa, and the balance position of the shaft neck gradually deviates from the center of the sliding bearing.

This article studies the lubrication characteristics of sliding bearings in gear pumps. The research results (such as oil film thickness, pressure distribution, etc.) can provide theoretical basis for the clearance, structural optimization, and material selection of sliding bearings, thereby optimizing their design and manufacturing processes. For gear pumps, the study analyzed the changes in the

balance position of the shaft neck, which helps optimize and improve the radial clearance in gear pump design and manufacturing, thereby reducing leakage and improving volumetric efficiency.

Funding

The research is supported by the Henan Provincial Key Research and Development Special Project (251111220200), Natural Science Foundation of Henan Province Project (252300420446), and Henan Provincial Science and Technology Research Project (242102220026).

Conflicts of interest

The authors declare no conflict of interest.

Data availability statement

The article data may be obtained from the corresponding author by making a reasonable request.

Author contribution statement

Shuai Wang and Zhenchao Hao for writing the manuscript and simulation analyses. Weifeng Han and Juntao Liu contributed to the data and overall structure planning of the article. Geqiang Li, Yunda Liu and Yiwei Wu contributed to the simulation modelling.

References

1. S. Guo, J. Chen, Y. Lu, Y. Wang, H. Dong, Hydraulic piston pump in civil aircraft: current status, future directions and critical technologies, Chin. J. Aeronaut. **33** (2020) 16–30
2. L. Liang, L. Wang, J. Wang, The compensation for nonlinear friction of DDVC flange-type rotary vane steering gear, Plos One. **13** (2018) e0207018
3. Z. Wang, Q. Liang, J. Zhang, J. Gao, Z. Zhang, Control strategy of direct-drive pump-controlled hydraulic system based on adaptive backstepping method, J. Mech. Electr. Eng. **41** (2024) 1376–1385
4. K. Huang, G. Han, Y. Xiong, Z. Cheng, M. Sang, Design and fluid analysis of the microsegment gear tooth profile for pump operating at high speed and high pressure, P. I. Mech. Eng. E-J. Pro. Mech. Eng. **59** (2023) 1–16
5. T. Zhang, The trend and challenges of high-speed hydraulic pump technology in the era of electrification-According to the recording and compilation of expert xu bing's report from Zhejiang University, Hydraulics Pneumatics Seals **42** (2022) 103–107
6. G. Li, L. Zhang, W. Han, Profile design and displacement analysis of the low pulsating gear pump, Adv. Mech. Eng. **10** (2018) 1–11
7. Y. Zhou, Y. Ci, Temperature rise of journal bearing of the high-speed circular arc gear pump, P. I. Mech. Eng. C-J. Mech. Eng. Sci. **234** (2020) 1492–1499
8. J. Fu, S. Zhong, K. Luo, X. Liu, S. Wei, Analysis of aeroengine fuel pump hydrostatic journal bearing lubrication and parameter influence, J. Propul. Technol. **44** (2024) 1–21
9. C. Gu, X. Meng, D. Zhang, Y. Xie, Transient analysis of the textured journal bearing operating with the piezoviscous and shear-thinning fluids, J. Tribol. **139** (2017) 051708
10. J. Tacconi, S. Shahpar, A. King, J. Olufeagba, R. Khan, I. Sant, M. Yates, Elasto-hydrodynamic model of hybrid journal bearings for aero-engine gear fuel pump applications, J. Tribol. **144** (2022) 031604
11. G. Gu, Y. Guo, Z. Wang, Analysis of influence of clearance ratio on bearing characteristics of sliding bearing of fuel pump, Mach. Tool Hydraulics. **40** (2022) 142–147
12. Y. Xie, Y. Wang, X. Song, J. Zhao, Lubrication analysis of seawater lubricated UHMWPE bearing with different acceleration and deceleration modes, Lubr. Eng. **44** (2019) 77–82
13. T. Zhang, Y. Wang, C. Xu, L. Wang, Influence of fluctuation in supply pressure on the elastohydrodynamic lubrication (EHL) of water-lubricated hybrid journal bearing, J. Mech. Transm. **41** (2017) 10–14+26
14. A. Solghar, F. Brito, J. Claro, S. Nassab, An experimental study of the influence of loading direction on the thermohydrodynamic behavior of twin axial groove journal bearing, P. I. Mech. Eng. J-J. Eng. Tribol. **225** (2011) 245–254

Cite this article as: Shuai Wang, Zhenchao Hao, Weifeng Han, Juntao Liu, Geqiang Li, Yunda Liu, Yiwei Wu, Research on lubrication characteristics of sliding bearings in circular arc gear pumps under variable operating conditions, Manufacturing Rev. **12**, 11 (2025), https://doi.org/10.1051/mfreview/2025007